南京航空航天大学

论文集

（二〇〇七年）第11册

能源与动力学院

（第1分册）

南京航空航天大学科技部编

二〇〇八年三月

能源与动力学院

023 系

目录

序号	姓名	职称	单位	论文题目	刊物、会议名称	年、卷、期	类别
1	张靖周 谭晓茗	正高 中级	023 023	Experimental study on flow and heat transfer characteristics of synthetic jet driven by piezoelectric actuator	Science in China E	2007.50.2	
2	张靖周 谭晓茗	正高 中级	023 023	压电驱动自耦合射流流动和换热特性实验研究	中国科学E辑	2007.37.3	
3	张靖周 单勇 李立国	正高 中级 正高	023 023 023	直升机排气系统用波瓣喷管引射-混合式红外抑制器研究	航空学报	2007.28.1	
4	王奉明 张靖周 王锁芳	硕士生 正高 正高	023 023 023	不同形状扰流柱矩形通道内流动特性研究	航空学报	2007.28.1	
5	唐正府 张靖周	博士生 正高	023 023	利用喷管引射和旋翼下洗的红外抑制器特性研究	南京航空航天大学学报	2007.39.3	
6	唐正府 张靖周	博士生 正高	023 023	直升机红外抑制器两种进气方式下的实验研究	推进技术	2007.28.3	
7	唐正府 张靖周 王先炜 刘强	博士生 正高 正高 中级	023 023 602所 602所	排气系统与尾机身一体化红外抑制器实验分析	航空动力学报	2007.22.2	
8	余业珍 张靖周 杨卫华	博士生 正高 副高	023 023 023	突片射流冲击冷却换热特性的实验	航空动力学报	2007.22.9	
9	杨成风 张靖周 李伟	博士生 正高 硕士生	023 023 023	仿螺旋肋化通道流动换热特性的数值研究	工程热物理学报	2007.28.S2	
10	王磊 张靖周 杨卫华 李延斌	硕士生 正高 副高 硕士生	023 023 023 023	冲击/发散冷却气膜冷却效率的实验研究	工程热物理学报	2007.28.S2	
11	宋双文 杨卫华 胡好生 张靖周	博士生 副高 副高 正高	023 023 608所 023	冲击＋逆向对流＋气膜冷却传热特性的研究	航空动力学报	2007.22.9	
12	宋双文 胡好生 杨卫华 张靖周	博士生 副高 副高 正高	023 608所 023 023	扰流柱对叶片尾缘对流换热特性的影响	航空动力学报	2007.22.10	
13	李建华 宋双文 杨卫华 张靖周	博士生 正高 副高 正高	023 608所 023 023	不同结构肋化通道对流换热特性的试验	航空动力学报	2007.22.10	
14	杨卫华 李永康 张靖周 马国锋	副高 副高 正高 硕士生	023 中航一集团 023 023	突片作用下气膜冷却效率的试验研究	航空动力学报	2007.22.3	

目录

序号	姓名	职称	单位	论文题目	刊物、会议名称	年、卷、期	类别
15	张义宁 王家骅 刘鸿 张靖周	中级 正高 博士生 正高	023 023 023 023	多循环脉冲爆震发动机工作过程中的延迟时间研究	航空动力学报	2007.22.2	
16	张义宁 王家骅 何小民 张彭岗 韩启祥 张靖周	中级 正高 副高 博士生 副高 正高	023 023 023 023 023 023	爆震室压力测量可靠性试验	航空动力学报	2007.22.10	
17	范育新 王家骅 李建中 张义宁	副高 正高 中级 中级	023 023 023 023	脉冲爆震发动机气动阀性能分析	航空动力学报	2007.22.1	
18	范育新 王家骅 李杨	副高 正高 学士	023 023 023	PDE在模拟冲压进气条件下的台架推力修正	航空动力学报	2007.22.10	
19	范育新 王家骅 曹梦源	副高 正高 学士	023 023 023	脉冲爆震发动机供油自适应规律研究	航空动力学报	2007.22.11	
20	宫继双 范育新 王家骅	硕士生 副高 正高	023 023 023	汽油/空气两相多循环扇形PDE试验研究	中国航空学会第十四届燃烧与传热传质学术交流会	2007	
21	李红红 刘勇	硕士生 副高	023 023	基于详细反应机理的二维模型燃烧室中碳黑颗粒尺寸分布数值模拟	中国工程热物理学会燃烧学术年会	2007	
22	颜应文 赵坚行 张靖周	中级 正高 正高	023 023 023	燃烧室污染物生成大涡模拟模型的研究	航空动力学报	2007.21.1	
23	颜应文 赵坚行 张靖周 刘勇	中级 正高 正高 副高	023 023 023 023	大涡模拟模型燃烧室燃烧性能计算	中国航空学会第十四届燃烧与传热传质学术交流会	2007	
24	党新宪 赵坚行 吉洪湖	博士生 正高 正高	023 023 023	试验研究双旋流器头部燃烧室几何参数对燃烧性能影响	航空动力学报	2007.22.10	
25	张海涛 赵坚行	硕士生 正高	023 023	带隔热屏加力燃烧室热态流场计算	航空动力学报	2007.22.8	
26	蔡文祥 赵坚行	博士生 正高	023 023	带圆筒头部火焰筒两相燃烧流场及性能计算	推进技术	2007.28.2	
27	蔡文祥 赵坚行	博士生 正高	023 023	双头部燃烧室两相燃烧流场数值研究	工程热物理学报	2007.28. 增刊2	
28	胡好生 赵坚行 钟建平 蒋荣伟 尹美芝	博士生 正高 正高 副高 中级	023 023 608所 608所 608所	一种新颖的燃烧室出口温度场调试方法	航空动力学报	2007.22.8	
29	黄海明 赵坚行	硕士生 正高	023 023	数值模拟纵向隔热屏加力室热态流场	航空动力学报	2007.22.11	
30	李井华 赵坚行	博士生 正高	023 023	数值分析二级涡流器环形燃烧室的燃烧性能	航空动力学报	2007.22.8	

目录

序号	姓名	职称	单位	论文题目	刊物、会议名称	年、卷、期	类别
31	李井华 赵坚行 常海萍	博士生 正高 正高	023 023 023	双级涡流器环形燃烧室整体流场数值模拟	南京航空航天大学学报	2007.39.6	
32	谭晓茗 张靖周	中级 正高	023 023	压电驱动狭缝喷口自耦合射流流动特性研究	中国机械工程	2007.18.21	
33	谭晓茗 张靖周	中级 正高	023 023	Experiment on flow characteristics of synthetic jet driven by piezoelectric membrane	Transactions of NUAA	2007.24.3	
34	谭晓茗 张靖周	中级 正高	023 023	高校工科专业课课堂教学方法浅议	中国科技教育	2007.9	
35	张勃 罗明东 黄伟	中级 博士生 博士生	023 023 023	尾向可见明火大宽高比矩形喷管红外辐射特性实验研究	航空动力学报	2007.22.12	
36	张勃 吉洪湖	中级 正高	023 023	圆转矩形大宽高比收敛喷管过渡型面及喷管口形式对射流掺混特性的影响	航空动力学报	2007.22.3	
37	张勃 吉洪湖 罗明东 黄伟 蔡旭	中级 正高 博士生 博士生 硕士生	023 023 023 023 023	宽高比对尾向可见明火矩形喷管红外抑制特性影响研究	航空动力学报	2007.22.11	
38	罗明东 吉洪湖 黄伟 蔡旭 高潮	博士生 正高 博士生 硕士生 副高	023 023 023 023 023	用FTIR光谱仪测量排气系统中红外光谱辐射强度的方法	航空动力学报	2007.22.9	
39	罗明东 吉洪湖 黄伟	博士生 正高 博士生	023 023 023	非加力涡轮发动机排气系统红外辐射强度的数值计算	航空动力学报	2007.22.10	
40	罗明东 吉洪湖 黄伟 蔡旭 高潮	博士生 正高 博士生 硕士生 副高	023 023 023 023 023	涡扇发动机二元喷管的红外光谱辐射特性实验	推进技术	2007.28.4	
41	罗明东 吉洪湖 黄伟 蔡旭 张勃 高潮	博士生 正高 博士生 硕士生 中级 副高	023 023 023 023 023 023	二元喷管热喷流的红外光谱辐射特性实验	推进技术	2007.28.2	
42	罗明东 吉洪湖 黄伟 蔡旭 高潮	博士生 正高 博士生 硕士生 副高	023 023 023 023 023	轴对称喷管与后机身组合结构的红外特性实验	南京航空航天大学学报	2007.39.3	
43	李彬 吉洪湖 江义军 李锋	博士生 正高 正高 中级	023 023 624所 624所	燃烧室冲击-逆向对流-气膜冷却特性的数值研究	航空动力学报	2007.22.3	

目录

序号	姓名	职称	单位	论文题目	刊物、会议名称	年、卷、期	类别
44	李彬 吉洪湖 江义军	博士生 正高 正高	023 023 624所	冲击-发散冷却火焰筒浮动瓦片三维壁温计算分析	航空动力学报	2007.22.3	
45	袁艳平 吉洪湖 杜雁霞	博士后 正高	023 023 解放军理工大学	低压差驱动下中等半径比内轴高旋圆柱间流量的数值分析	润滑与密封	2007.32.1	
46	袁艳平 吉洪湖 王健 高久好	博士后 正高	023 023 工程兵科研一所	中等半径比内轴高旋圆柱间湍流场的大涡模拟	润滑与密封	2007.32.2	
47	白花蕾 吉洪湖 李娜 王亚龙	硕士生 正高 博士生 本科生	023 023 023 023	动静态下指式密封泄漏特性的实验研究	中国航空学会第十四届燃烧与传热传质学术交流会	2007	
48	宫禹 吉洪湖	硕士生 正高	023 023	外涵进气对发动机热喷流实验台流场均匀性的影响	南京航空航天大学第九届研究生学术会议	2007	
49	李建中 王家骅 范育新 张义宁 张靖周	中级 正高 副高 中级 正高	023 023 023 023 023	煤油/空气脉冲爆震发动机激波反射起爆研究	工程热物理学报	2007.28.2	
50	李建中 王家骅	中级 副高	023 023	煤油/空气脉冲爆震发动机强化燃烧装置	航空动力学报	2007.22.4	
51	赵承龙	正高	退休	运行状态下太阳热水系统热性能测试方案	能源研究与利用	2007.4	
52	何明鉴	正高	退休	课堂教学要注意的几个关键点	南京航空航天大学学报（社科版）	2007.9.2	

Science in China Series E: Technological Sciences

Experimental study on flow and heat transfer characteristics of synthetic jet driven by piezoelectric actuator

ZHANG JingZhou† & TAN XiaoMing

College of Energy and Power Engineering, Nanjing University of Aeronautics and Astronautics, Nanjing 210016, China

To investigate the flow and heat transfer characteristics of a synthetic jet driven by piezoelectric actuator, experimental investigation utilizing particle image velocimetry, hot-wire anemometer and infrared camera was carried out. The results show that: (1) At the jet orifice exit, pairs of vortexes are generated, broken down and merged together periodically, forming a steady jet within a several slot width from distance near the orifice exit. And during the development, the synthetic jet spreads rapidly along the minor axis direction of the orifice. While along the major axis direction, the synthetic jet contracts firstly and then spreads slowly. (2) Excitation frequency forced on the actuator has a great effect on the synthetic jet flow field. There are two resonance frequencies at which the mean velocity and vorticity of the synthetic jet are maximized, especially at the higher resonance frequency. The resonance frequency values obtained by the experiment are lower than the theoretical values. (3) Similarly to the common jet impingement, the convective heat transfer coefficients at the target surface impinged by the synthetic jet also take on up-down tendency varying with the jet-to-surface spacing increment. But the jet-to-surface spacing ratio for optimum cooling achievement is greater and the cooling action region is wider than the former, indicating that the synthetic jet introduces a stronger entrainment and more vigorous penetration in the surrounding fluid.

synthetic jet, impinging cooling, flow, heat transfer

The synthetic jet is a jet-like mean fluid motion formed by time-periodic, alternate suction and ejection of fluid through an orifice bounding a small cavity, by the time periodic motion of a diaphragm that is built into one of the walls of the cavity (Figure 1). The diaphragm is forced to oscillate, with fluid being expelled through the orifice as the diaphragm moves upwards. The flow separates at the edge of the orifice, inducing a vortex ring that moves outwards under its own

Received January 26, 2005; accepted October 12, 2006
doi: 10.1007/s11431-005-0006-1
†Corresponding author (email: zhangjz@nuaa.edu.cn)
Supported by the National Natural Science Foundation of China (Grant No. 50276028)

momentum. When the diaphragm moves downwards to entrain fluid into the cavity, the vortex ring is sufficiently distant from the orifice that it is virtually unaffected by the entrainment of the fluid into the cavity. Thus, over a single period of oscillation of the diaphragm, whilst there is zero net mass-flux into or out of the cavity, there is also a non-zero mean momentum flux. This momentum flux is, effectively, a jet that has been synthesized from the coalescence of a train of vortex ring of the ambient fluid. Due to the zero-net-mass-flux nature, which eliminates the need for plumbing, the synthetic jet is regarded as a novel concept for active flow control applications including jet vectoring, flow separation control, and boundary layer control. It is also potentially attractive for the enhanced heat transfer application since the synthetic jet is a highly pulsating flow, being contributed to a stronger entrainment and more vigorous penetration in the surrounding fluid.

Previous studies have covered the formation and development of the synthetic jet[1,2], the numerical simulation on the flow field of the synthetic jet[3−6], the performance of the synthetic jet actuator[7−10] and the application of the synthetic jet actuator[11,12]. The concept of using synthetic jets for heat transfer is relatively new, especially, with little or no attention given to the heat transfer enhancement by the synthetic jet impingement. In the present study, the flow and heat transfer characteristics of a synthetic jet driven by piezoelectric actuator were experimentally investigated utilizing particle image velocimetry, hot-wire anemometer and infrared camera.

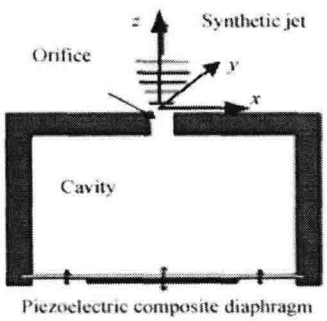

Figure 1 Schematic of synthetic jet actuator.

1 Experiment setup

The synthetic jet actuator for this experiment is shown in Figure 2, and is composed of a closed cylindrical cavity (inner diameter D = 30 mm, height H = 5 mm), in which one of the ends is covered by a flexible actuator diaphragm (thickness δ = 0.2 mm). A rigid wall (thickness δ = 1 mm) with a slot orifice (width b=0.5 mm, length l=10 mm) covers the other end. The actuator diaphragm consists of a thin, red copper sheet on which a piezoelectric ceramic disk (PZT-5) is bonded. The diameter of the red cooper sheet is 30 mm and its thickness is 0.1 mm. The diameter of the piezoelectric ceramic disk is 20 mm. The actuator diaphragm is excited with a variable frequency wave generator (YDS966A) whose output is amplified with a power amplifier (SA-750A). A square waveform was chosen to diver the piezo-element for the reason of the faster deflation of the actuator diaphragm when excited with a square wave.

The flow fields of the synthetic jet downstream the orifice were investigated without an opposing impingement wall. In this study, particle image velocimetry (PIV) and hot-wire anemometry (TSI model 1201-20) were used to acquire the synthetic jet flow field over a complete drive cycle. Independent measurements from two different techniques offer a cross check of the flow field data. Specifically, the instantaneous synthetic jet flow fields in a 2D plane along and across the slot orifice were measured by PIV. The hot-wire probe were set up to scan the time averaged velocity profile along the centerline of the synthetic jet flow.

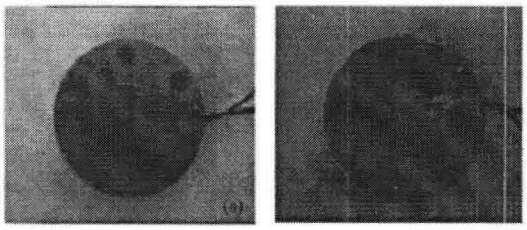

Figure 2 Synthetic jet actuators. (a) Jet orifice plate; (b) actuator diaphragm.

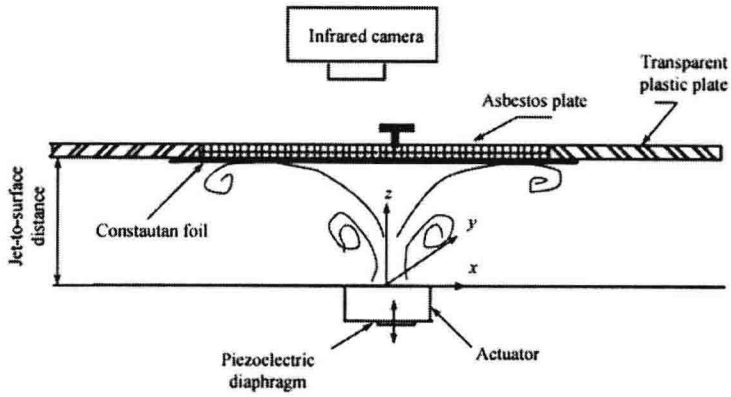

Figure 3 Schematic diagram of experimental system.

The experimental apparatus for the synthetic jet impingement is sketched in Figure 3. The impingement target is a thin constantan foil (100 mm wide, 150 mm long and 0.01 mm thick) held flat by a stiffening fixture on the transparent plastic plate. The foil is heated by passing an electric current through it and cooled by a synthetic jet directed perpendicular to it. The temperature distribution on the rear face of the foil (the opposite side of jet impingement) were measured by an infrared camera (TVS-2000MK) which works at speed of 30 frames per second, and the revolution of the temperature is –20°C—200°C. To make the object thermal image be detected by the infrared camera, a viewing window in the transparent plastic plate was made, with 50 mm wide and 70 mm long. When the foil being heated, the viewing window is covered with a thick asbestos plate. Once the temperature field on the impinging target was steady, the asbestos plate was taken out and the temperature distribution inside the viewing window was than measured by the infrared camera. The heating process was monitored by three thermo-couples fixed on the foil.

In fact, since the Biot number $Bi = hs/\lambda$ (where s and λ are the thickness and thermal conductivity of the foil, respectively) is much less than unity, the temperature can be considered practically uniform across the foil thickness. So the convective heat transfer coefficient on the target surface is evaluated as

$$h = \frac{Q - Q_s}{A(T_s - T_j)}, \tag{1}$$

where T_s is the target temperature, T_j is the synthetic jet temperature (may be regard as am-

bient temperature T_a), A is the effective area of heating foil, Q is the input power imposing on heating foil, Q_s are the heat losses including radiation and natural convection from impinging target.

$$Q_s = Q_r + Q_c, \tag{2}$$

here Q_r is radiation loss, Q_c is natural convection loss. They are estimated according to heat transfer basic theory[13].

$$Q_r = \varepsilon\sigma(T_w^4 - T_a^4), \tag{3a}$$

$$Q_c = h_c(T_w - T_a), \tag{3b}$$

where ε is the outer surface emissivity of the transparent plastic plate, σ is the Stefan-Boltzman constant, h_r is the natural convection coefficient. T_w is the average temperature on the transparent plastic plate, measured from five thermo-couples fixed on the outer surface of the transparent plastic plate. Differences between considering and neglecting heat losses are generally on the order of 2%—6%.

2 Flow visualization of synthetic jet

Figure 4 shows the time sequence of the instantaneous flow field generated by the synthetic jet actuator from a slot orifice operating at a frequency of 1000 Hz and an input voltage of 175 V for one period of oscillation of the membrane. The pictures of flow field, taken in a 2D plane along the minor axis direction of the slot orifice (x-z plane) were shown in Figure 4(a), illustrate the formation-development process of the vortex ring. As the membrane oscillates, the ambient air is alternately drawn into and expelled out from the cavity orifice. When the fluid is expelled out from the slot orifice, a shear layer forms at the slot edges, and the vorticity in the shear layer rolls up ambient air to form pairs of counter-rotating vortices. Some traces of the previous vortex pair are still discernible in the middle downstream and the emerging turbulent jet is visible farther downstream. In subsequent images, the new vortex pair undergoes the transition and development, shedding into the surrounding fluid, wrapping around the cores of the primary vortices and dissipating downstream. Because of periodic formation of new vortex pairs in the slot orifice, continuous momentum is replenished to the downstream to maintain the quasi-continuity of the synthetic jet.

Figure 4(b) shows pictures of flow field taken from the side of slot-length (y-z plane). Because the orifice length is too big comparing with the vortex size, pairs of vortices could not be seen near the slot exit but a narrow strip vortex. As the narrow strip vortex moves away from the slot, it breaks down into a series of vortices and diffuses into the surrounding fluid.

As may be seen in Figure 5, the PIV vector plots are superimposed over vorticity plots that were generated for time-average using the data obtained by PIV analysis. The physical size of each plot is 30 mm wide and 30 mm high. The bottom border of the plots coincides with the actuator orifice. The vorticity is defined as

$$\Omega = \nabla \times V, \tag{4}$$

here Ω is the vorticity, V is the velocity vector.

Closer to the jet exit plane (z/b=10—15), the vorticity appears the maximum, and at this normal position, the magnitude of the centerline velocity also appears the biggest. This behavior

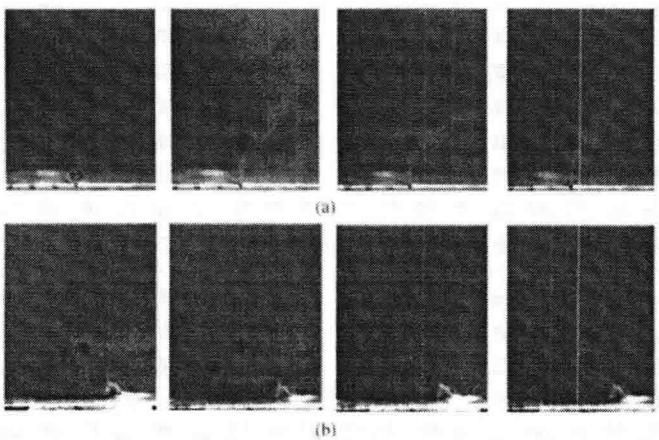

Figure 4 Time sequence of the flowfield visualization of synthetic jet. (a) The section plane along slot-width direction (x-z plane); (b) the section plane along slot-length direction (y-z plane).

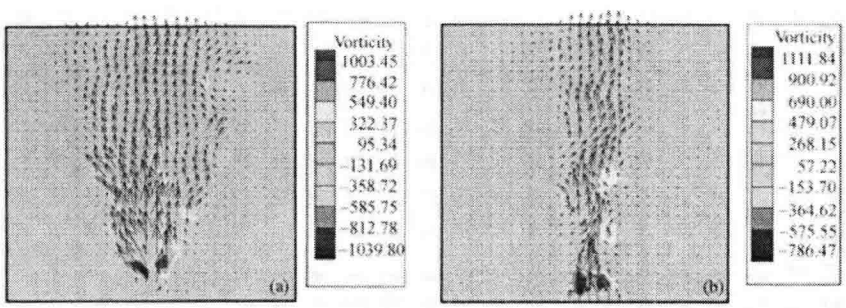

Figure 5 Velocity vectors and vorticity distributions of synthetic jet. (a) The section plane along slot-width direction; (b) the section plane along slot-length direction.

perhaps is the indication that the steady synthetic jet is already developed. From this normal section plane on, the vorticity is gradually diffused into the surrounding fluid (the vorticity values are low). It is important to note that the diffusion process in the section plane along slot-width direction is virtually different from that in the section plane along slot-length direction. A remarkable difference is that the synthetic jet spreads rapidly in the minor axis direction of the orifice, while in the major axis direction, the synthetic jet contracts firstly and then spreads slowly. A reasonable cause for this phenomenon is attributed to the un-even vorticity distribution of the narrow strip vortex, referring to the vorticity is relatively weaker in the vicinity of orifice ends. When the synthetic jet is developed downstream, the vortex pairs with lower vorticity are drawn into the vortex pairs with higher vorticity in the middle orifice, forcing the synthetic jet contracts. As the synthetic jet is developed further downstream, the surrounding fluid is rolled up, causing the synthetic jet to propagate at a certain speed.

3 Exciting resonance frequency

It may be expected that the velocity output from the actuator reaches a peak value when it is ex-

cited at its resonance frequency. Assuming that the vibrating diaphragm is modeled as a circular disk, rigidly clamped at its edge, the solution to this problem is well documented[14], and the first two resonance frequencies, $f_{1,2}$, are given by

$$2\pi f_{1,2} = K_{1,2}\sqrt{\frac{4Et^3}{3(1-\upsilon^2)m_a D^4}}, \tag{5}$$

where $K_{1,2}$=10.2 and 21.3, respectively; E is Young's modulus (107.9 Mpa); t is the thickness of actuator disk (0.1 mm); ν is Poisson's ratio (0.35); m_a is the mass per unit area of actuator disk (density is 8900 kg/m^3); D is the disk diameter (30 mm). The first two resonance frequencies of the actuator were computed using eq. (5), based on the mechanical properties of the steel disk alone. They are f_1=548 Hz and f_2=1144 Hz.

The time-averaged centerline velocities at different normal distances away from the jet orifice were measured by hot-wire anemometry. The results are presented in Figure 6, where the time-averaged velocity is plotted with respect to the excitation frequency. Two resonance frequencies of f_1=340 Hz and f_2=1000 Hz are easily identified. It is evident that the actuator produces fairly high velocities even when operated off-resonance and the synthetic jet could not be formed under some frequencies. These results are consistence with the measurement by PIV. It is also seen that the centerline velocity accelerates to a maximum at a normal distance of z/b=10—15 under excitation resonance frequency of 1000 Hz.

The discrepancy between the experimental and analytical values (especially at the lower resonance frequency) may be related to the interference introduced by the piezoelectric disk that was bounded at the center of the steel disk. The vibrating mode and the mechanical properties simplified in the analysis are somewhat different from the real case. And another reason is that the vibrating system should be more complicated than the analytical model, being composed of vibrating diaphragm, cavity and fluid inside cavity. Therefore the inertial action of the fluid inside cavity maybe induces negligible influence on the resonance frequency of the actuator. It is should be noted that the excitation resonance phenomenon is common for the synthetic jet actuator, but the values of the excitation resonance frequency are relationship to the structure of the actuator.

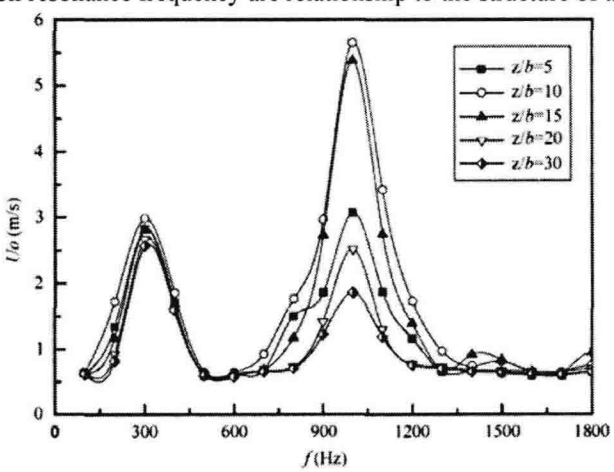

Figure 6 Mean centerline velocity at different excitation frequencies.

Analyzing the flow field features of the synthetic jet in details, it is found that pairs of vortex are generated, broken down and merged together periodically, forming the continue jet at one normal distance near the jet orifice (z/b is about 6). And then during the development of the synthetic jet, it spreads rapidly in the orifice minor axis direction. While in the major axis direction, the synthetic jet contracts firstly and then spreads slowly. This transition position occurs in the range of z/b=10—15, where the centerline velocity of the synthetic jet flow accelerates to a maximum value.

4 Heat transfer on impingement target

Figure 7 shows the temperature distributions on the constant heat-flux (1000 W/m^2) heating foil surface under the impingement of the synthetic jet actuated at a frequency of 1000 Hz and a voltage of 175 V. In the thermal images, each plot is 50 mm wide and 75 mm length in the physical size and the horizontal direction coincides with the major axis direction of the slot orifice.

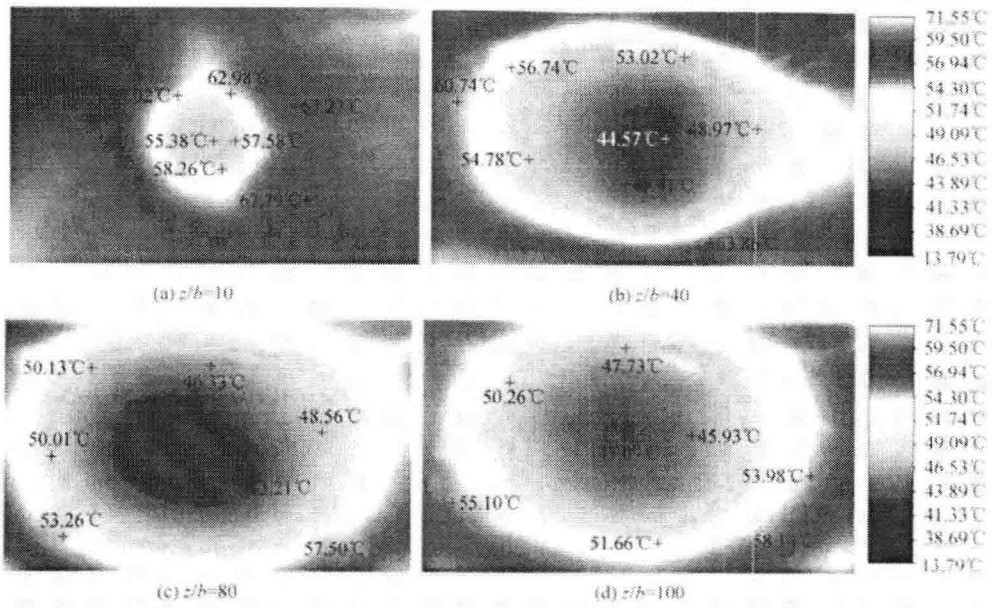

Figure 7 Temperature contour of heated plate at different impinging distances (q=1000 W/m^2).

As the non-dimensional jet-to-surface distance z/b varies from 10 to 100, the temperature distributions on the target take on different features. In the case of z/b=10, the isothermal contours appear to be approximately circular. With the jet-to-surface distance far away from the jet orifice, the isothermal contours appear obviously elliptical, and the cooling area enlarges as also as the minimal temperature value decreases. Although the major axis direction of the elliptical isothermal contours coincides with the orifice length direction in general, it is interest to find that the major axis direction for the core cooling area is in the direction of the orifice minor axis direction when z/b=40. Once the non-dimensional jet-to-surface distance reaches to 80, the cooling action by the synthetic jet behaves the optimum.

In the case of z/b=10, corresponding to the transition position of the synthetic jet, although the

centerline velocity of the synthetic jet flow accelerates to a maximum value in this normal distance, the sufficient diffusion of the synthetic jet does not occur, therefore the action region of the synthetic jet is confined on the impinging target. It is worth noting that the flow field measurement was conducted in the exception of the impinging target. Once a solid plate is placed near the jet orifice, the steady synthetic jet flow should not formed, for the reason is that the vortex ring generated in the vicinity of the orifice is not sufficiently distant from the orifice that it is virtually affected by the entrainment of the fluid into the cavity. As far as the heat transfer characteristics by the impingement cooling is concerned, z/b=10—15 is not the optimum non-dimensional jet-to-surface distance for achieving the best cooling performance. On the other hand, if the jet-to-surface distance is too big, the intensity of the synthetic jet should decay severely, resulting in a poor cooling action on the impinging target. In the present study, the optimum non-dimensional jet-to-surface distance is 80.

According to the velocity vectors and vorticity distributions of synthetic jet (Figure 5), the diffusion capacity of the synthetic jet is significantly advantage in the minor axis direction of the orifice in the middle of downstream. Refer to the position z/b=40, the profile of the synthetic jet is wider in the minor axis direction of the orifice than that in the major axis direction, resulting in that the major axis direction for the core cooling area is in the direction of the orifice minor axis direction. The features of the temperature distribution on the heating foil surface are consistent with the flow characteristics of the synthetic jet.

The local heat transfer coefficient distribution profiles with respect to the orifice minor and major axis directions, respectively, are presented in Figure 8. All the profiles are similar to each other that the local heat transfer coefficient value is the maximum at the impingement stagnation and decrease with the increase of x/b or y/b. Similarly to the common jet impingement, the convective heat transfer coefficients at the target surface impinged by the synthetic jet also take on up-down tendency varying with the jet-to-surface spacing increment, but the jet-to-surface spacing ratio for optimum cooling achievement under the impingement of the synthetic jet is greater than that of common jet impingement[15]. Another notable feature is that the cooling region under the impingement of the synthetic jet is wider than that of common jet impingement. The decay rate of the local heat transfer coefficient in the regions away from the impingement stagnation is obviously weaker compared to the common jet impingement. It is indicated that the synthetic jet introduces a stronger entrainment and more vigorous penetration.

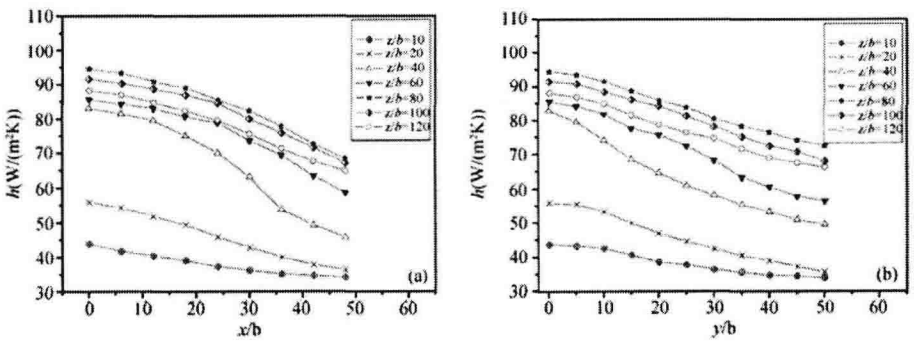

Figure 8 Local heat transfer coefficient distributions at different jet-to-surface distances. (a) Minor axis direction of jet orifice; (b) major axis direction of jet orifice.

5 Conclusions

(1) At the jet orifice exit, pairs of vortexes are generated, broken down and merged together periodically, forming a steady jet within a several slot width from distance near the orifice exit. And during the development, the synthetic jet spreads rapidly along the minor axis direction of the orifice. While along the major axis direction, the synthetic jet contracts firstly and then spreads slowly. This transition position occurs in the range of z/b=10—15, where the centerline velocity of the synthetic jet flow accelerates to a maximum value.

(2) Excitation frequency forced on the actuator has a great effect on the synthetic jet flow field. There are two resonance frequencies at which the mean velocity and vorticity of the synthetic jet are maximized, especially at the higher resonance frequency. The resonance frequency values obtained by the experiment are lower than the theoretical values. With the exception that the vibrating mode and the mechanical properties simplified in the analysis are somewhat different from the real case, the inertial action of the fluid inside cavity maybe induces negligible influence on the resonance frequency of the actuator.

(3) The features of the temperature distribution on the heating foil surface are consistent with the flow characteristics of the synthetic jet. Similarly to the common jet impingement, the convective heat transfer coefficients at the target surface impinged by the synthetic jet also take on up-down tendency varying with the jet-to-surface spacing increment. But the jet-to-surface spacing ratio for optimum cooling achievement is greater and the cooling action region is wider than the former, indicating that the synthetic jet introduces a stronger entrainment and more vigorous penetration in the surrounding fluid.

1 Smith B L, Glezer A. The formation and evolution of synthetic jets. Physics of Fluids, 1998, 10(9): 2281—2297
2 Luo X B, Li Z X, Guo Z Y. Analysis of the machanism of synthetic jet formation (in Chinese). J Tsinghua Univ (Sci. & Tech.), 2000, 40(12): 86—89
3 Linda D K, John F D. Numerical simulation of synthetic jet actuators. AIAA Paper 97-1924, 1997
4 Rizzerta D P, Visbal M R, Stanek M J. Numerical investigation of synthetic-jet flow fields. AIAA Journal, 1999, 37(8): 919—927
5 Goldstein D B. Two-dimensional synthetic jet simulation. AIAA Paper 2000-0406, 2000
6 Tan X M, Zhang J Z. Numerical simulation of impingement cooling by synthetic jet (in Chinese). J Engin Thermphys, 2004, 25(4): 646—648
7 Mallinson S G. The operation and application of synthetic jet actuators. AIAA Paper 2000-2402, 2000
8 Guy Y, McLaughhlin T E, Morrow J A. Velocity measurements in a synthetic jet. AIAA Paper 2000-0118, 2000
9 Luo X B, Li ZX, Guo Z Y. Design and analysis of synthetic jet actuated by piezoelectric actuator (in Chinese). J Funct Mater Devices, 2001, 7(2): 116—120
10 Tan X M, Zhang J Z. Numerical investigation of the influence factors and flow characteristics for a synthetic jet (in Chinese). J Aerospace Power, 2005, 20(5): 836—840
11 Smith B L, Glezer A. Vectoring and small-scale motions effected in free shear flows using synthetic jet actuators. AIAA Paper 97-0213, 1997
12 Amitay M, Honohan, Trautman M, Glezer A. Modification of the aerodynamic characteristics of bluff bodies using fluidic actuators. AIAA Paper 97-2004, 1997
13 Yang S M, Tao W Q. Heat Transfer (in Chinese). Beijing: Advanced Education Press, 1998
14 Young W C. Roark's formulas for stress & strain. New York: McGraw-Hill, 1989
15 Downs S J, James E H. Jet impingement heat transfer: A literature survey. ASME Paper 87-HT-35, 1987

中国科学 E辑：技术科学
2007年 第37卷 第3期：431~437
http://www.scichina.com

《中国科学》杂志社
SCIENCE IN CHINA PRESS

压电驱动自耦合射流流动和换热特性实验研究

张靖周* 谭晓茗

(南京航空航天大学能源与动力学院，南京 210016)

摘要 采用三维粒子图像测速仪、热线风速计和红外热像仪对狭缝喷口自耦合射流的流动特征和冲击靶板的对流换热特征进行了实验研究. 结果表明，在紧邻喷口的法向距离内，涡对周期性地生成、破碎和融合，在某个法向距离上形成较为稳定的连续性射流；随着自耦合射流的发展，呈现在喷口短轴方向急剧向两侧扩展、而在喷口长轴方向先收缩后缓慢扩展的流动特征. 激发器存在两个谐振频率，使得自耦合射流的速度和涡量比较大，其中高频谐振频率效果更好；实验得到的两个谐振频率在数值上与理论分析有一定差异，低频谐振频率相对差值更大. 与常规射流冲击冷却相比，自耦合射流冲击作用下的靶面对流换热系数同样具有随冲击间距增大而先逐渐增大、后逐渐衰减的变化趋势，但最佳冲击间距值却明显高于常规射流，而且自耦合射流的作用范围大，表明自耦合射流具有强的夹带能力和穿透能力.

关键词 自耦合射流 冲击冷却 流动 传热

在一个开缝或孔的腔体上利用压电材料或薄膜的周期振动使缝隙处产生一系列向外扩展的非定常涡环，这一系列的涡环对外流的作用类似于一股射流，称为自耦合射流(图1). 由于自耦合射流能够对附面层和主流产生重要的影响，甚至可以改变主流的方向，因此被认为是一种全新的流动控制概念而引起越来越广泛的重视. 同时由于自耦合射流流动具有脉动性，比相同雷诺数下常规的连续射流具有更强的夹带能力，所以在强化换热方面也具有潜在的应用前景. 目前针对自耦合射流的形成机理和演变过程[1,2]、自耦合射流的数值模拟[3~6]、自耦合射流激发器的性能研究[7~10]和应用研究[11,12]等方面已经开展了众多基础性的研究工作，但是将自耦合射流用于强化传热的研究在国内外还相对缺乏. 本文通过实验研究对压电驱动单膜片激励的自耦合射流的流动和换热特性进行研究，进一步揭示自耦合射流的流动特征和冲击靶板的对流换热特征.

收稿日期: 2006-03-24; 接受日期: 2006-10-12
国家自然科学基金资助项目(批准号: 50276028)
* E-mail: zhangjz@nuaa.edu.cn

1 实验系统

实验中采用圆柱形腔体自耦合射流激发器(图 2), 腔体直径 D = 30 mm, 腔体高度 H = 5 mm; 腔体顶面为射流孔板, 厚度为 1 mm, 狭缝喷口宽度 b = 0.5 mm, 长度 l = 10 mm; 腔体底面为压电膜片, 厚度为 0.2 mm, 由 PZT-5 型压电陶瓷片和紫铜膜片黏结而成, 紫铜片直径为 30 mm, 厚度为 0.1 mm, 压电陶瓷片直径为 20 mm.

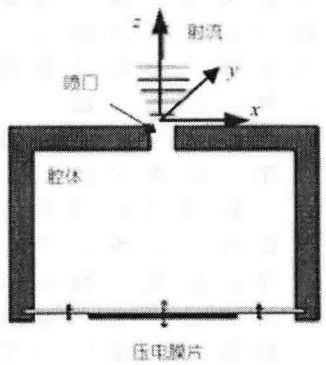

图 1 自耦合射流原理简图

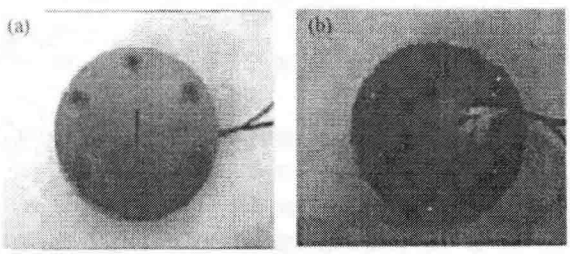

图 2 激发器实验件
(a) 射流孔板; (b) 激发器膜片

激发器驱动系统包括: YDS966A 型信号发生器, 用于输出合适的波形; SA-750A 型功率放大器, 用于输出功率信号. 在作用于同样阻抗和功率因子的电路上, 方波输入功率最大, 驱动激发器时将会使激发器获得的机械能最大, 从而压电膜片的振幅最大, 所以实验中采用方波输入[11].

利用三维粒子图像测速仪 PIV 对自耦合射流激发器在不同激励频率下发展过程中的流场进行测试, 同时利用热线风速仪对自耦合射流的时均速度进行测量. 自耦合射流的流场测试是在未放置冲击靶板的情况下进行的.

在自耦合射流冲击冷却实验中, 冲击靶板为厚度 0.01 mm 的康铜加热膜片(长 150 mm, 宽 100 mm), 加热膜压贴在厚度为 10 mm 聚丙烯塑料板上. 为了便于红外热像仪拍摄温度图像, 在塑料板上开设 70 mm×50 mm 的测量窗口. 加热时, 测量窗仍采用石棉块覆盖, 一旦在自耦合射流作用下的冲击靶面的温度场达到热稳定状态, 取出石棉块, 用红外热像仪对暴露在测量窗口的冲击靶板背面的温度图像迅速进行拍摄. 热稳定状态通过固定在加热膜上的 3 对热电偶监测, 如图 3.

由于毕渥数 $Bi = hs/\lambda$ 远小于 1, 其中 s 和λ分别为加热膜片的厚度和导热系数, 因此可以认为在膜片厚度上的温度是一致的, 即冲击靶板正面和背面的温度值几乎没有差异.

冲击靶面的对流换热系数定义为

$$h = \frac{Q - Q_s}{A(T_s - T_j)}, \tag{1}$$

式中 T_s 为冲击靶面温度; T_j 为自耦合射流温度, 可以视为环境温度; Q 为电热膜片的加热功率, A 为电热膜片的面积; Q_s 为加热膜散热损失, 包括辐射换热损失 Q_r 和自然对流换热损失 Q_c, 即